A METHOD FOR QUALITATIVELY MAPPING THE FLOOD PHYSICAL VULNERABILITY OF RESIDENTIAL AREAS

To-Uyen Thi Doan[1, *], Ariyo Kanno[2], Koichi Yamamoto[2], Tsuyoshi Imai[2], Takaya Higuchi[2], Masahiko Sekine[2]

[1]*Ho Chi Minh City University of Natural Resources and Environment, 236B Le Van Sy street, Tan Binh district, Ho Chi Minh city, Viet Nam*

[2]*Graduate School of Sciences and Technology for Innovation, Yamaguchi University, 2-16-1 Tokiwadai, Yamaguchi 755-8611, Japan*

[*]Email: *touyen892@gmail.com*

Abstract. Mapping flood physical vulnerability is spatially limited because it requires input data such as building structures and mat

erials, which are unavailable on large spatial scales. In this study, we propose a new method for qualitatively evaluating the flood vulnerability of residential areas in the context of the exposure and resilience to flood hazard on large spatial scales. This method utilizes the possible correlations between the structural physical vulnerability and residential types obtained from the statistical classifications of multispectral satellite images. Because multispectral classification is well-established as an inexpensive technique for automatically classifying land cover types over wide areas, our method is feasible and efficient for mapping the physical vulnerability of residential areas. As a case study, we present an application of the proposed approach to the Thach Ha district, Ha Tinh province, Vietnam, using the Japanese type 2 Advanced Visible and Near Infrared Radiometer (AVNIR-2) images and Phased Array type L-band Synthetic Aperture Radar (PALSAR) images captured by the Advanced Earth Observing Satellite (ADEOS).

Keywords: qualitative evaluation; physical vulnerability; flood mapping; residential areas; multispectral classification.

Classification numbers: 3.5.2, 2.9.

1. INTRODUCTION

In recent decades, the number of natural floods has increased in the context of climate change, causing extensive loss and damage to residential areas. Between 1975 and 2000, among all the natural disasters, floods impacted the most number of people in Asia and caused the most damage in Europe [1]. Flood risk depends on the following location-specific factors: (i) hazardous event, (ii) vulnerability, and (iii) elements-at-risk [2]. Flood risk can be assessed traditionally as the combined product of the probability of and damage caused by the hazard and vulnerability [3]. In 2016, a holistic participatory approach for flood risk assessment presented both quantitative and qualitative methods to generate an alternative flood risk map; however, it was limited to providing details on a small spatial scale [4].

Vulnerability is defined as the susceptibility of a community to the impact of a hazardous event. Because vulnerability depends on numerous components, it can change rapidly, and generally, explain the reason for the same hazardous event having a different effect on the various elements-at-risk [5]. The different types of variability found are: physical, social, economic, and environmental vulnerabilities [6]. Flood physical vulnerability can be determined as the degree of loss of the physical infrastructure and population owing to flooding. The physical conditions comprise of the exposure to the flood hazard (location relative to the hazard and environmental surrounding), susceptibility of the elements-at-risk (the constructions in the flooded areas), and resilience (adjustments, preparation) depending on the self-adaptation of the local residents [7, 8, 9]. Among the construction materials used to determine the physical vulnerability, certain materials have a higher sensitivity to floods than earthquakes [5]. To determine the flood physical vulnerability, some previous research studies delineated flood areas to assess the exposure to the flood hazard using optical and radar images [10, 11]. The susceptibility and resilience to flood hazard are commonly obtained from detailed fieldwork data and mapping exercises with local residents [4, 8].

Some calculation methods have been proposed for determining the physical vulnerability of residential areas; however, they require data such as the building structure and materials for obtaining the susceptibility of the elements-at risk, which are unavailable on large spatial scales. This is because buildings have different structures and materials and so, generally lack spatial ordering, which makes it easier to evaluate such buildings directly from high-resolution imagery. Manual identification of detailed structural types has been applied in participatory mapping approaches [4, 5, 6, 8]. However, it is an expensive and time-consuming process, also requiring finely detailed information, which is available only at small spatial scales.

Multispectral satellite remote sensing is an efficient technique for inexpensively observing a wide area. Although it cannot directly observe the structure or material of each house, it is capable of automatically classifying land cover types, including residential areas [12]. It has the potential for application to vulnerability mapping if a correlation between the structure or material and different land cover classes in the residential areas can be established. Kang, Su, and Chang demonstrated that the damages caused to land uses and building types are not identical after the same flood event [13].

The objective of this research is to propose a simple approach to qualitatively evaluate the physical vulnerability of different residential areas to flood disasters. This study uses the correlation between the house physical vulnerability and land-cover classification obtained from contemporary multispectral satellite imagery. We demonstrate the capability of this method using the Advanced Visible and Near Infrared Radiometer type 2 (AVNIR-2/ALOS) images and Phased Array type L-band Synthetic Aperture Radar (PALSAR) images captured over the Thach Ha district, Ha Tinh province, Viet Nam.

2. PROPOSED APPROACH

2.1. Qualitative evaluation of flood physical vulnerability

First, an unsupervised classification of the land cover is performed using one or more multispectral satellite image(s) of the target region. The classification parameters are adjusted so that the residential areas are categorized into multiple classes.

Next, *in situ* land cover measurements at discrete locations in each land cover class are recorded as the ground truth data for calibration. At this stage, the land cover characteristics for

each class and inundated information at each GPS point are clarified. The locations of the residential areas, structures, and materials in the different classes are observed in detail and their physical vulnerabilities are quantitatively evaluated.

Next, a supervised land-cover classification is performed for achieving a better accuracy, using the same satellite image(s) and a majority of the ground truth points for training. The land cover classes can include permanent water, vegetation, bare lands, and residential areas. Here, the classes should be modified so that each residential area belongs to a uniform class.

Subsequently, the relationships between the physical vulnerabilities of the residential area classes and their subsidiary sample houses are investigated. The established correlations can be used to qualitatively evaluate the physical vulnerability of each residential area in the target region.

2.2. Analyzing flood physical vulnerability in terms of exposure and resilience

First, the exposure is determined by combining the floodplains that occurred in some recent years in the research area. The combination of floodplains yields the probability of flood hazard. To this end, each floodplain is extracted by comparing the radar images before and during the flood event. A radar image is well-known to be an effective satellite image in comparison with other optical images for extracting flooding areas [11].

In addition, the height of the flood water affected by the geography should be analysed because vulnerability strongly depends on the status of the water level. The digital elevation model (DEM) is useful for identifying the geographic features of the research area. The DEM is used to classify the various geographic features. The water level in the different geographic features in a floodplain is determined by interviewing the local population and taking samples.

Finally, the spatial distribution of the resilience to flood in the residential area is determined from the participatory information on the adaptability of the local residents to a flood or method for the mitigation of a flood.

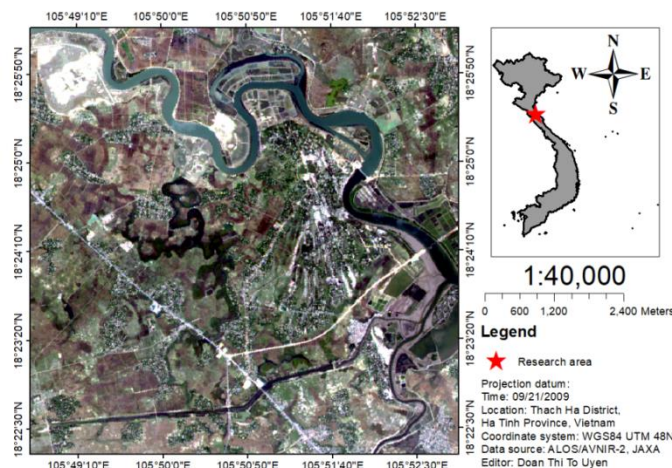## 3. DEMONSTRATION METHOD

3.1. Study area

Figure 1. Location of the study area in the Thach Ha district, Ha Tinh province, Viet Nam.

The study area is in central Viet Nam, in a flat area of the delta of the Sot river, Thach Ha district, Ha Tinh province, Viet Nam (Figure 1). In this area, a large 100-yr-flood was caused by the 2010 La Nina in the autumn season between 4–16 October 2010.

Choosing to analyse the severest flood that occurred in 2010 as the study area offers certain conveniences for our demonstration method. First, because this area has a flat topography, the backscattering errors of satellite images that are affected by the topographic conditions are reduced to a minimum. This supports easier and more exact observance of the land cover and floodplains with a simple calibration. Second, under the condition of geographic stability and characteristics of the fluid dynamics of the water run-off to lower regions, the floodplain of the severest flood event with the highest rainfall can cover the floodplains of other flood events.

3.2. Unsupervised classification

An unsupervised classification was performed using the K-means method [14] on a multispectral ALOS/AVINIR-2 image with three visible bands and a single near-infrared band, acquired on 21 September 2009 in the autumn season prior to the 2010 flood. Following radiometric calibration and geometric correction, the image was used as the input for land-cover classification. The samples of the desired class numbers were tested with the K-means classification numerous times to identify the land cover classes in the study area. It was possible to vary the number of classes between a minimum of five and a maximum of ten. Categorizing the land coverage into nine classes established the correct number of multiple residential area classes when collating the classified results with a high-resolution optical image from Google Earth. A comparison with Google Earth imagery was not required for an input image with a sufficiently high resolution because the residential areas could be confidently identified.

3.3. Acquisition of ground truth data

From the fieldwork, 215 random ground truth points of the land cover characteristics and flooding information were recorded in the autumn season after the 2010 flood to identify the nine classes. We selected the number of ground truth points in each land cover type based on the area ratio of the land cover type from the unsupervised classification. All the land cover types were sampled during the fieldwork. The ground truth points for studying the land cover characteristics were randomly separated into 128 training and 87 testing points. We collected additional training areas for performing supervised classification by determining the uniform land-use area around each training point using images from Google Earth. Fifty two ground truth points were in residential areas for which the structures or materials and their flood damages were specified. We classified them into groups based on the similarity in the structure or material characteristics and then calculated the physical vulnerability of each building type.

3.4. Supervised classification of land coverage

A multispectral supervised classification was processed with two types of data: same ALOS/AVINIR-2 images and ground truth areas. Both the maximum likelihood estimation (MLE) and textural features were used for the classification; the latter facilitates modifying each residential area so that it belongs to a uniform class and improves the classification accuracy.

The MLE [15] was employed with a combination of four original bands and three appropriate textural bands for the multispectral supervised classification. The training areas were supported to create a region of interest (ROI) required for the MLE.

In the textural classification, heterogeneous characteristics were observed between the sparse and dense residential areas when comparing the AVNIR-2 and Google Earth images. For the land-coverage classification, textural features, mean, standard deviation, and coefficient of variation were obtained for a rectangular neighbourhood to extract the differences in the image band grey tones [16]. Textural feature trials were established in each image band and rectangle neighbourhood to choose the most effective textural applications for the classification. We identified these as the blue band, coefficient of variation (7×7), green band, mean (7×7), red band, and standard deviation (7×7).

After the classification, the testing points were utilized to generate a classification error matrix. The overall accuracy and Kappa index (κ) were calculated as the indicators of the accuracy with equal weight of variables [17].

3.5. Physical vulnerability calculation

Table 1. Matrix to assess the physical (structural) vulnerability index of a house in natural hazards [18].

		WEIGHT	**Structural degree**		
			Low	*Medium*	*High*
			1	3	5
Structural characteristics	*Walls*	15	block, brick metallic structure	adobe	cardboard, light wood, plastic, bamboo
	Roof, materials	10	concrete slab	galvanized sheeting, cement tiles	straw, plastic brick tiles
	Roof, inclination	5	very inclined	moderately inclined	low inclination
	Roof, support material	5	Steel structure, new, treated wood	old, non-treated wood	weights, stones
	Doors	1	metal, wood	small windows	large windows
	Windows	1	metal, wood	small glass	

Based on the model used by De León and Carlos (Table 1), we calculated the physical vulnerability of each house type observed during the fieldwork. The model assessed the physical vulnerability associated with the housing sectors based on the elements-at-risk of loss. In this model, the correlated matrix between the structural degrees (low, medium, and high) and house structures, walls, roof materials, roof inclination, roof support material, doors, and windows was established based on the characteristics of the structural materials. The structural vulnerability is calculated as follows:

$$V_{estruct} = \sum W_{ij} \quad \text{with} \quad W_{ij} = W_i \times W_j \tag{1}$$

where W_i and W_j are the weights of the structural characteristics in row i house structures and column j structural degrees, respectively, in the model correlation matrix, and $V_{estruct}$ is the calculated structural vulnerability. The maximum structural vulnerability is 185.

We converted $V_{estruct}$ to the physical vulnerability index (*PVI*) related to house sectors. *PVI* was calculated as the ratio of the house structural vulnerability and maximum structural vulnerability. The vulnerability is expressed on a scale from 0 (no damage potential) to 1 (highest damage potential).

$$PVI = V_{estruct} \div V_{estruct_{max}} \quad \text{with} \quad V_{estruct_{max}} = 185 \tag{2}$$

3.6. Qualitative evaluation of physical vulnerability of residential areas

We considered the correlation between the land-use classes and physical vulnerability by observing the frequencies of the structural physical vulnerabilities of different residential types. Finally, we qualitatively evaluated the physical vulnerability of different residential areas from the possible correlations.
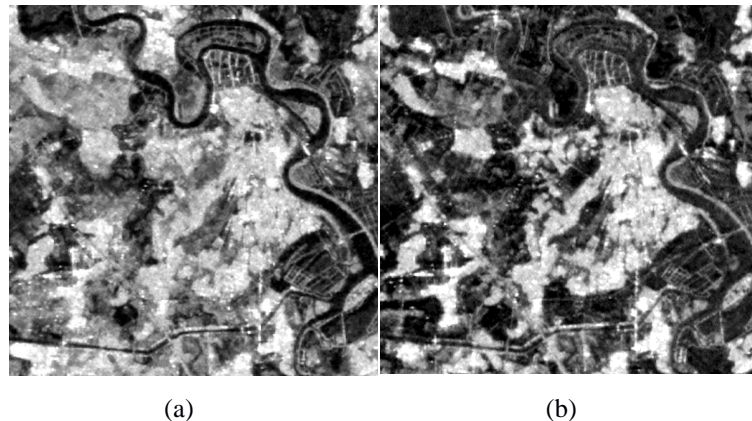
3.7. Determination of exposure to flood hazard

| (a) | (b) |

Figure 2. Backscatter images (a) before the flood acquired on 30 August, 2010 and (b) during the flood acquired on 15 October 2010. The data source was ALOS PALSAR, JAXA.

To extract the floodplain to determine the exposure, we quantitatively evaluated the difference in the backscattering coefficient before and during the flood event using two L-band radar satellite images (ALOS/PALSAR) acquired on 30 August 2010 and 15 October 2010 (Figure 2). The multi-temporal images have a homogeneous nadir angle resolution and were captured in the same geographical location. The images before and during the flood should be captured within a short period. This is to reduce the differences in the topography unrelated to the effects of the flood.

During pre-processing, speckle noise removal, conversion of the digital number (DN) to the backscatter coefficient, and geometric correction of the radar images need to be performed initially.

First, we decided to use double filters including Lee's filter (7 × 7) and low-pass filter (3 × 3) to remove the speckle noise in the PALSAR images. The double filter supported the minimization of the misinformation of the images. Subsequently, we transformed the DN of the pixel to the backscattering coefficient and corrected the geometry relevant to the study area [19].

Next, we obtained the absolute backscattering difference by subtracting the radar image captured during the flood from the image captured before the flood. The quantitative evaluation of the backscattering difference was analyzed in the inundated and non-inundated areas of each land cover type. We masked the value of the backscattering difference in permanent water to 0 dB to distinguish permanent water with inundated area. We classified the land covers into two groups of land surface: complex group with numerous impediments on the surface and rough group without impediments on the surface. In this step, the thresholds for the segmentation of the inundated and non-inundated areas in each land cover and land surface were realized. The presence of flooding was detected, which demonstrated effective floodplain extraction. After

that, we again compared the floodplain with the land cover map to remove the omission error in the inundated area.

Finally, during post-processing, the flooding information of the ground truth points was used to calculate the error matrix and Kappa index with equal weights for the inundated and non-inundated areas, leading to accurate segmentation.

3.8. Determination of resilience to flood

To identify the resilience, we designed a household survey with a questionnaire to collect the information from the local residents on the adaptation to and mitigation of the flood. The survey was only processed randomly at 72 households located in the inundated areas. Half of the households were in a dense residential area, and the other half were in a sparse residential area. The question required them to take some actions to adapt to or mitigate a flood; to rank the effectiveness of the actions, using six values ranging from 0 (no effect) to 5 (strong effect); and to list their protections for their constructions.

After collecting the participatory data, we determined six levels of constructed protection. The levels and their significance are as follows: level 0 (Non-protection), level 1 (Slightly improving the background height by soil and sand), level 2 (Moving properties to a safe place), level 3 (Significantly improving the background height by cement or reinforcing the roof and wall), level 4 (Mixing more than one solution to protect constructions), and level 5 (Rebuilding/Relocation of a house to a non-inundated area).

4. DEMONSTRATION RESULTS
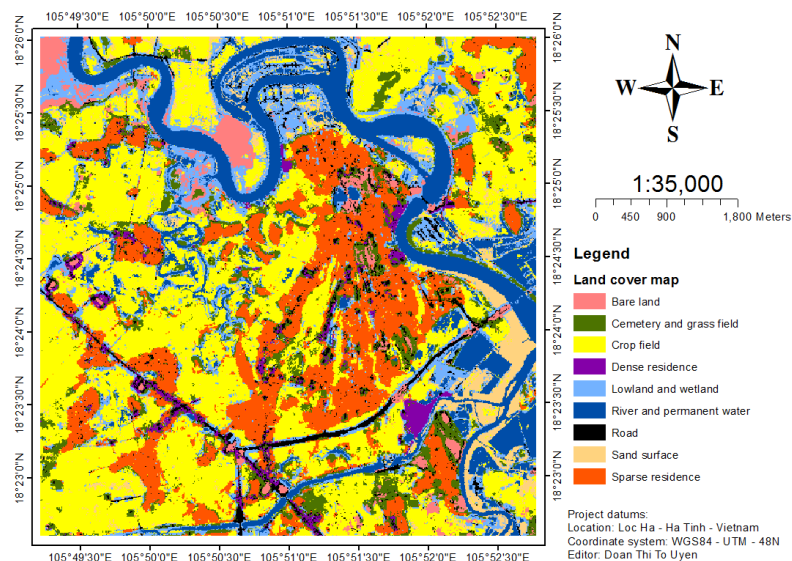
Figure 3. Spatial distributions of the nine land-cover classes in the Thach Ha district, Ha Tinh province, Viet Nam.

The spectral and textural classifications yielded the land-coverage spatial distribution with the nine land cover classes (Figure 3). Among these, two types of residential areas were

identified, dense and sparse, depending on the structural density and vegetation. The dense residential areas had densely built houses, whereas the sparse residential area had a mixture of sparsely built houses and dense trees in the house gardens. After the classifications, the overall classification accuracy based on the testing set of 87 ground truth points was found to be 85 %, with a κ-index of 0.833.

4.1. House types and their physical vulnerability

The 52 observed houses in the residential area were categorized into 13 types based on the house characteristics (Table 2). From house type 1 to 13, the strength of the structural materials decreased, so that the physical vulnerability correspondingly increased. Higher recorded vulnerabilities correlated with more serious damage.

Table 2. Thirteen house types in the research area categorized based on the *PVI* and house structure and material.

Type	Description	PVI	Damage and losses
1		0.36	Low flood level: walls were damp and broken. Medium flood level: there was slight building subsidence (< 4 cm). High flood level: small parts of the houses were destroyed.
2		0.37	Low flood level: there was slight yard and building subsidence. Medium flood level: walls and parts of the houses were broken and destroyed. High flood level: houses were unroofed and sloped slightly.
3		0.38	Low flood level: there was slight yard and building subsidence
4		0.42	Medium flood level: there was medium building subsidence (> 4 cm) and parts of houses were destroyed and unroofed.
5		0.42	Low flood level: there was slight yard and building subsidence and the walls were damp and broken. Medium flood level: there was medium building subsidence (> 4 cm) and parts of the houses were destroyed and unroofed. High flood level: large parts of the roofs were broken and unroofed.
6		0.42	High flood level: large parts of the roofs were broken and unroofed.
7		0.43	Low flood level: small parts of the roofs were unroofed, there was slight building subsidence, and there were broken walls. Medium flood level: roof and building structures were broken and the walls were partially damp and broken.

585

8		0.44	Medium flood level: the walls were partially damp and broken; houses were partially destroyed, unroofed, and sloped slightly; and there was strong building subsidence.
9		0.47	Low flood level: there were slight building subsidence and broken walls and the houses were partially unroofed.
10		0.47	Low flood level: there were slight building subsidence and broken walls and the houses were partially unroofed.
11		0.74	Medium flood level: large parts of the walls were destroyed, houses sloped strongly, and there was strong building subsidence.
12		0.82	Low flood level: large parts of the walls were destroyed, houses sloped strongly, and there was strong background subsidence.
13		0.88	Low flood level: houses were significantly destroyed and there was strong background subsidence.

*Note: Low flood level is 0–0.6 m; medium level is 0.6–1.3 m; high level is 1.3–3 m.

4.2. Qualitative evaluation of physical vulnerabilities of different residential areas
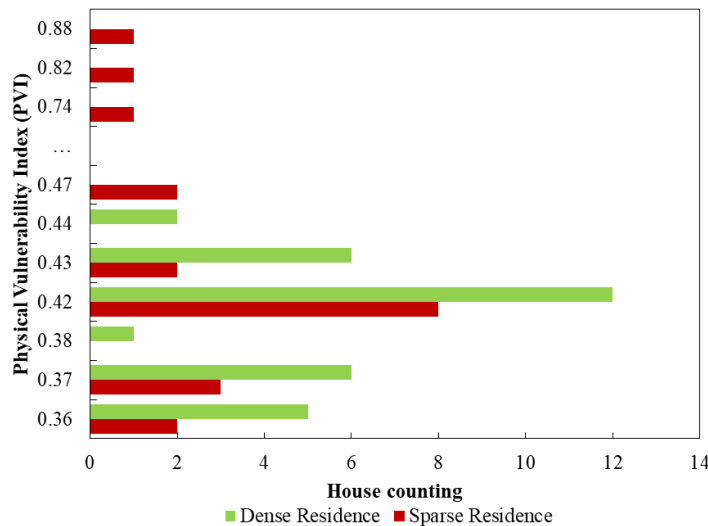

Figure 4. Distributions of the houses based on different vulnerabilities and residential areas in the Thach Ha district, Ha Tinh province, Viet Nam.

586

The correlation between the residential classes and physical vulnerability was established by comparing houses in different residential areas and the *PVIs* (Figure 4). Among the 52 houses, 20 were located in sparsely built areas and 32 were in densely built areas.

The results indicated an inverse correlation between the structural density and structure physical vulnerability of the study site: sparser residential areas had a higher flood physical vulnerability or weaker house structures or materials. Specifically, lower physical vulnerabilities, *PVI* from 0.36 to 0.44, were found in dense residential areas. We also found that abrupt high physical vulnerability values in house types 11, 12, and 13 with *PVIs* of 0.74, 0.82, and 0.88, respectively, only occurred in sparse residential areas.
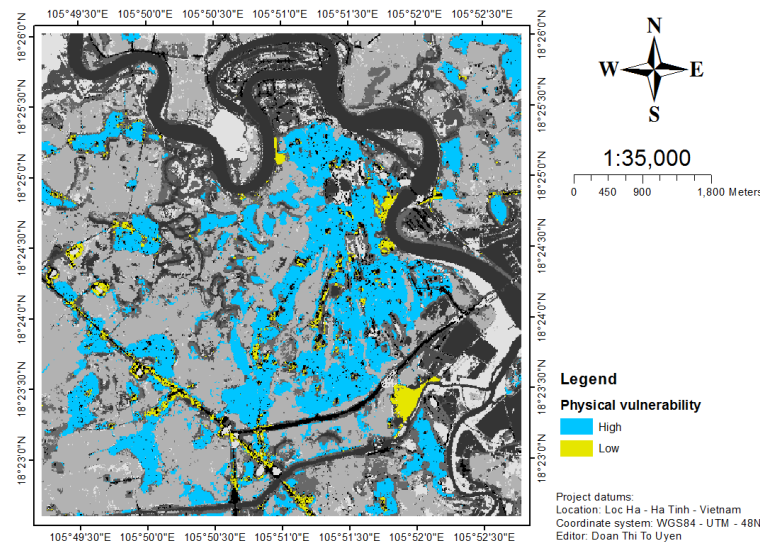

Figure 5. Estimated physical vulnerabilities of the residential areas in the Thach Ha district, Ha Tinh province, Viet Nam.

Finally, based on the correlation, the physical vulnerability was qualitatively evaluated by the land-cover classification (Figure 5). In this process, we found that more detailed residential classifications provided a more detailed distribution of the physical vulnerability.

4.3. Exposure to flood hazard

Figure 6 shows the backscattering difference for the land cover types. Figures 6a and b display the backscattering difference for a sparse residence and (cemetery and grass field), respectively, with complex surfaces. The backscattering difference for the bare land, sand surface, and crop field in the non-harvest season (Figures 6c, d, and e, respectively) corresponds to rough surfaces. We realize that on a rough surface, the backscattering difference for the non-inundated areas is larger than for the inundated areas; whereas the reverse occurs on complex surfaces.

Following the determination of the threshold values to segment the non-inundated and inundated areas in Figure 6, we extracted floodplains. The floodplains in both the rough and complex surfaces are shown (Figure 7).

From the quantitative analysis, we also observed that the backscattering intensity measured in dense residential areas was almost unchanged when comparing two satellite images captured

before and during the flood. This is because the satellite sensor cannot receive the original backscattering signals from a narrow water surface that is changed by crowded buildings and constructions. However, floods have occurred in some dense residential areas, using radar images to extract floods in densely populated areas has little effect.
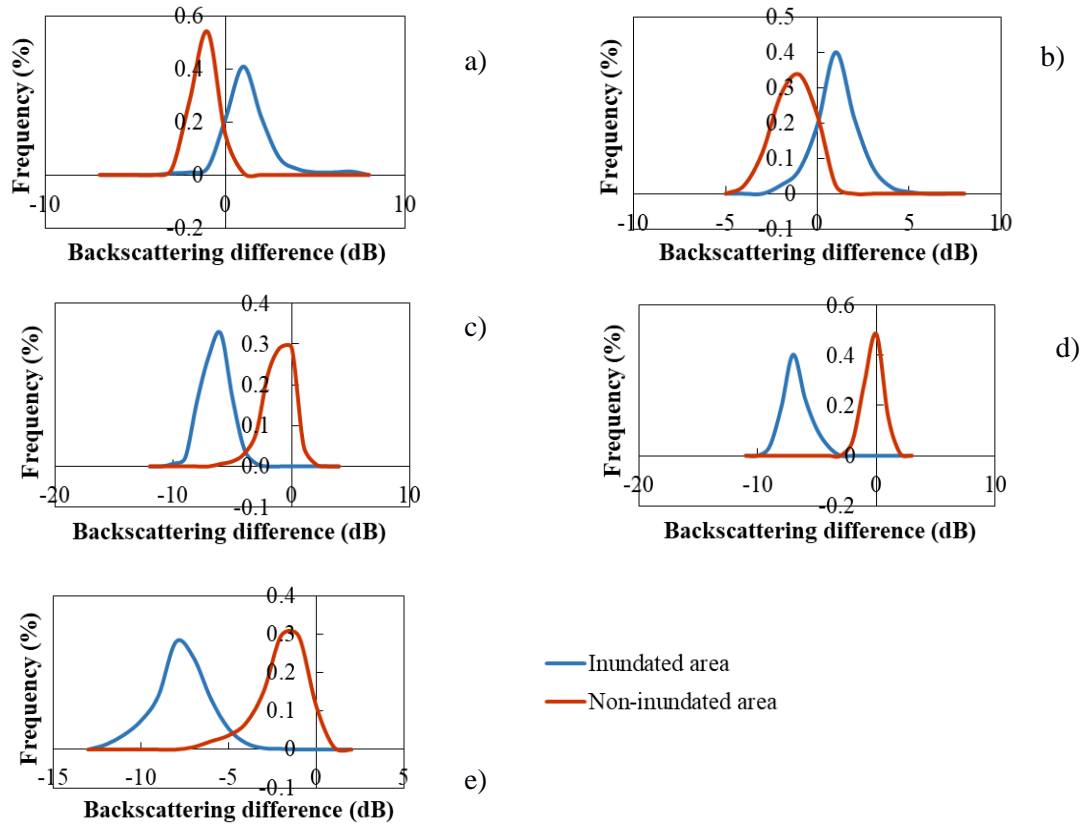

Figure 6. Backscattering difference of inundated and non-inundated areas: (a) Sparse residential area; (b) Cemetery and grass field; (c) Bare land; (d) Sand surface; (e) Crop fields in non-harvest season.
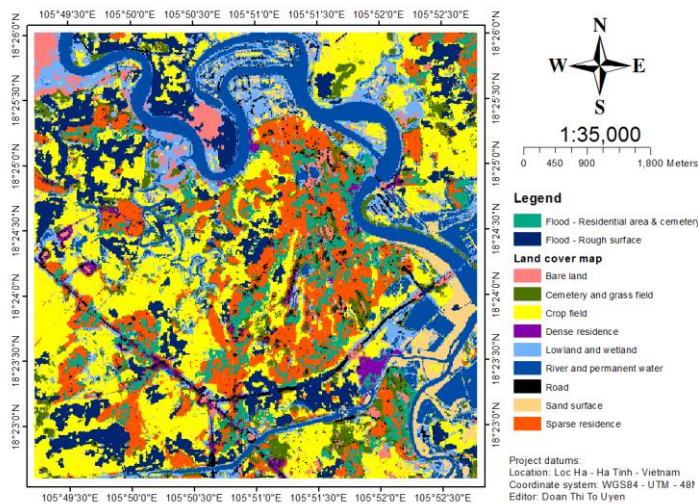

Figure 7. The floodplains in the rough and complex surfaces of the 2010 flood.

Finally, the error matrix and Kappa index were calculated for two inundated and non-inundated areas for each land cover. The accuracy of the segmentation shows that we attain the qualified accuracy when segmenting floodplains in the bare land (86 %), sand surface (95 %), crop field (89 %), cemetery/grass field (83 %), and sparse residential areas (90 %). In opposition, the accuracy and Kappa index of only 39 % and 0.14, respectively, for the segmentation of floodplains in dense residential area are low.

4.4. Resilience of local people to flood

Figure 8 shows the percentage of households in the sparse/dense residential area in each effective level that is conducted by the household survey. The figure presents the six levels of constructed protection according to the six values of the effectiveness of local people actions to adapt or mitigate the flood.
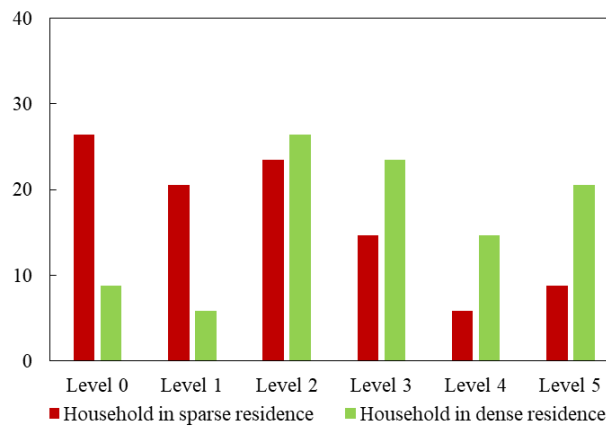

Figure 8. Percentage of number of households in each effective level of the solutions to protect constructions.

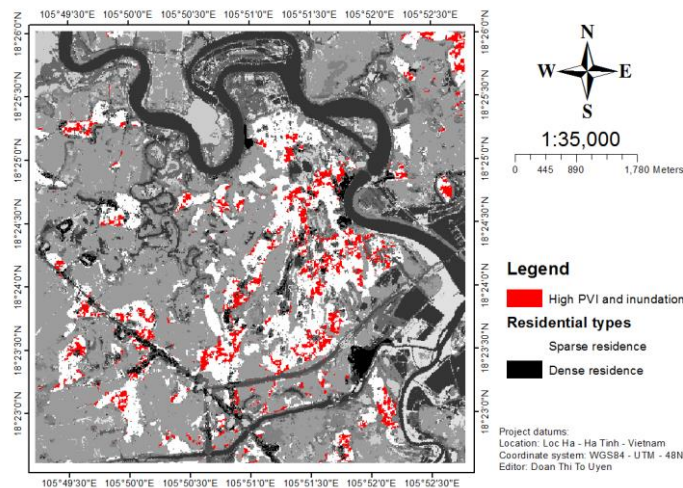## 4.5. Risky regions to flood hazard and suggestions to the government

Figure 9. Risky regions in study area.

The risky regions for flood hazard are identified in the analysis of the physical vulnerability in the context of the exposure and resilience to flood hazard. In our study, the risky areas were established by combining the high physical vulnerability, highest ability of inundation, and weakest resilience recorded in the study area (Figure 9). We observed that the risky areas are practically located in the sparse residential areas. The identification of risky regions yielded more detailed information on the vulnerability to the local government to provide timely guidance and attention to citizens when responding to a flood.

4. CONCLUSIONS

This study proposed a qualitative evaluation method of the structural vulnerability of residential areas using optical and radar satellite remote sensing. Specifically, we demonstrated that in residential areas where land-cover classifications correlated with house structures or materials, satellite images could provide a detailed land-cover classification. This would facilitate a qualitative evaluation of the physical vulnerability of residential areas. The advantage of this approach is the ability to automatically enhance the evaluation of the vulnerability and identify risky areas on a large spatial scale, which was unavailable in previous methods. The applicability and limitation of this approach should be investigated through additional case studies in different areas.

REFERENCES

1. ADRC. 20th Century [1901–2000] Asian Natural Disasters Data Book, 2002.

2. Ebert A., Kerle N., and Stein A. - Urban social vulnerability assessment with physical proxies and spatial metrics derived from air- and space borne imagery and GIS data, Natural Hazards **48** (2) (2007) 275-294.

3. Wisner B. - Turning knowledge into timely and appropriate action: Reflections on IDB/IDEA program of disaster risk indicators. BID/IDEA Programa de Indicadores para la Gestión de Riesgos, Universidad Nacional de Colombia, Manizales, 2003.

4. Vojinovic Z., Hammond M., Golub D., …, Michael Abbott - Holistic approach to flood risk assessment in areas with cultural heritage: a practical application in Ayutthaya, Thailand, Natural Hazards **81** (2016) 589-616.

5. Müller, A., Reiter J., and Weiland U. - Assessment of urban vulnerability towards floods using an indicator-based approach - a case study for santiago de chile, Natural Hazards and Earth System Sciences **11** (8) (2011) 2107-2023. Retrieved from https://search.proquest.com/docview/1027223059?accountid=41859.

6. van Westen C. J., Alkema D., Damen M. C. J., Kerle N., and Kingma N. C. - Multi-hazard risk assessment: Distance education course, United Nations University–ITC School on Disaster Geo-information Management (UNU-ITC DGIM)*,* 2011.

7. Pelling M. - What determines vulnerability to floods; a case study in Georgetown, Guyana, Environment and Urbanization **9** (1) (1997) 203-226.

8. Haase D. - Participatory modelling of vulnerability and adaptive capacity in flood risk management, Natural Hazards **67** (2013) 77-97.

9. UNESCO-IHE. 2017. "Flood Vulnerability Indices (FVI)".

    http://unihefvi.free.fr/vulnerability.php

10. Sanyal J., and Lu X. X. - Remote sensing and GIS-based flood vulnerability assessment of human settlements: a case study of Gangetic West Bengal, India, Hydrological Processes **19** (2005) 3699- 3716.

11. Rimba A. B., Setiawati M. D., Sambah A. B., and Miura F. - Physical Flood Vulnerability Mapping Applying Geospatial Techniques in Okazaki City, Aichi Prefecture, Japan. Urban Science **1** (1) (2017) 7.

12. Kettig R. L., and Landgrebe D. A. - Classification of multispectral image data by extraction and classification of homogeneous objects, IEEE Transactions on Geoscience Electronics **14** (1) (1976) 19-26.

13. Kang J. L., Su M. D., and Chang L. F. - Loss functions and framework for regional flood damage estimation in residential area, Journal of Marine Science and Technology **13** (3) (2005) 193-199.

14. Hartigan J. A., and Wong M. A. - Algorithm AS 136: A k-means clustering algorithm. Journal of the Royal Statistical Society, Series C (Applied Statistics **28** (1) (1979) 100-108.

15. Richards J. A. - Remote Sensing Digital Image Analysis, Springer-Verlag, Berlin, 1999.

16. Haralick R. M., and Shanmugam K. - Textural features for image classification, IEEE Transactions on Systems, Man, and Cybernetics **3** (6) (1973) 610-621.

17. Congalton R. G. - A review of assessing the accuracy of classifications of remotely sensed data, Remote Sensing of Environment **37** (1991) 35-46.

18. De León V., and Carlos J. - Vulnerability: a conceptional and methodological review, United Nations University Institute for Environment and Human Security, 2006.

19. Dewantoro M. D. R., and Farda N. M. - ALOS PALSAR Image for landcover classification using pulse coupled neural network (PCNN), International Journal of Advanced Research in Computer and Communication Engineering **1** (5) (2012) 289-294.